T.Le Meute, F.Bertrand, N.Seiler, E.Merle, D.Heuer

[Left hand page running head is author's name in Times New Roman 8 point bold capitals, centred. For more than two authors, write AUTHOR et al.]

MODELISATION OF A POSTULATED REACTIVITY INSERTION IN A GENERATION IV MOLTEN SALT REACTOR

T. Le Meute[1,3], F. Bertrand[1], N. Seiler[2], E. Merle[3], D. Heuer[3]

[1]CEA, DES, DER, SESI, F-13108 Saint-Paul-lez-Durance, France
[2]CEA, DES, DTN, SMTA, F-13108 Saint-Paul-lez-Durance, France
[3]CNRS, IN2P3, LPSC / Grenoble INP, PHELMA / UGA, F-38000 Grenoble, France

lemeute@lpsc.in2p3.fr, frederic.bertrand@cea.fr, nathalie.marie@cea.fr, elsa.merle@lpsc.in2p3.fr, daniel.heuer@lpsc.in2p3.fr

Abstract

The reference MSFR (Molten Salt Fast Reactor) is a 3000 MWth molten salt reactor. In most molten salt reactors, such as the MSFR, the fissile and fertile materials are dissolved in a circulating salt that acts both as fuel and as coolant (the fuel transports heat). The physical state of the fuel permits to consider draining as a way to mitigate hypothetical accidents. Moreover, a large-scale compaction cannot occur in such a core because, contrary to the solid fuel in a Fast Neutron Reactor, the fuel is nearly in its most compact geometry. This concept can be operated in the Th/U cycle and a fluoride salt or in the U/Pu cycle and a chloride salt. The goal of this work is to study the MSFR behaviour in case of a postulated reactivity insertion. In order to study the consequences of extreme reactivity insertions, the first objective is to study slow reactivity insertions to verify the efficiency of the draining of the liquid core. Then, in the case of extreme reactivity insertion, at the beginning of the transient, the salt cannot freely expand and the neutronic feedback is reduced. When the temperature of the salt rises, some vapor could be formed in the fuel, the vaporization of the salt could then lead to a quick expansion of the vaporized fluid. To perform these studies, we developed two independent codes. The first one, described in the present paper together with some associated studies and results, is being developed to study slow reactivity insertion. The second code, still under development, aims at calculating pressure and vaporization transient. The calculation tool seems to correctly represent the evolution of the calculated physical quantities and the mesh convergence is easily reached. This is encouraging for the continuation of this work to achieve the chaining with the fast phase calculation tool.

INTRODUCTION

This work is carried out in the framework of the European project SAMOSAFER. The aim of this project is to develop and demonstrate safety barriers for the MSFR [1] in accidental operation with some associated code developments and experimental validations. This work focuses on an accidental operation caused by postulated reactivity insertion. To study the accidental operation, a calculation tool has been developed in this work and the aim of this paper is to present this calculation tool and its application.

The phenomenological tree of this transient is represented in Fig.1. The reactivity insertion will lead to a degraded state of the core, to a power and temperature increase. This temperature increase will, thanks to the Doppler effect, make the reactivity decrease, and will also lead to an expansion of the salt. If the expansion of the salt is slow enough, the expansion feedback can act and decrease the reactivity: this is the slow phase. If the reactivity inserted is high enough, this expansion will trigger the draining of the core. It should be mentioned that because of the presence of an expansion tank, the beginning of this draining has no impact on the reactivity of the core.

T.Le Meute, F.Bertrand, N.Seiler, E.Merle, D.Heuer

[Left hand page running head is author's name in Times New Roman 8 point bold capitals, centred. For more than two authors, write
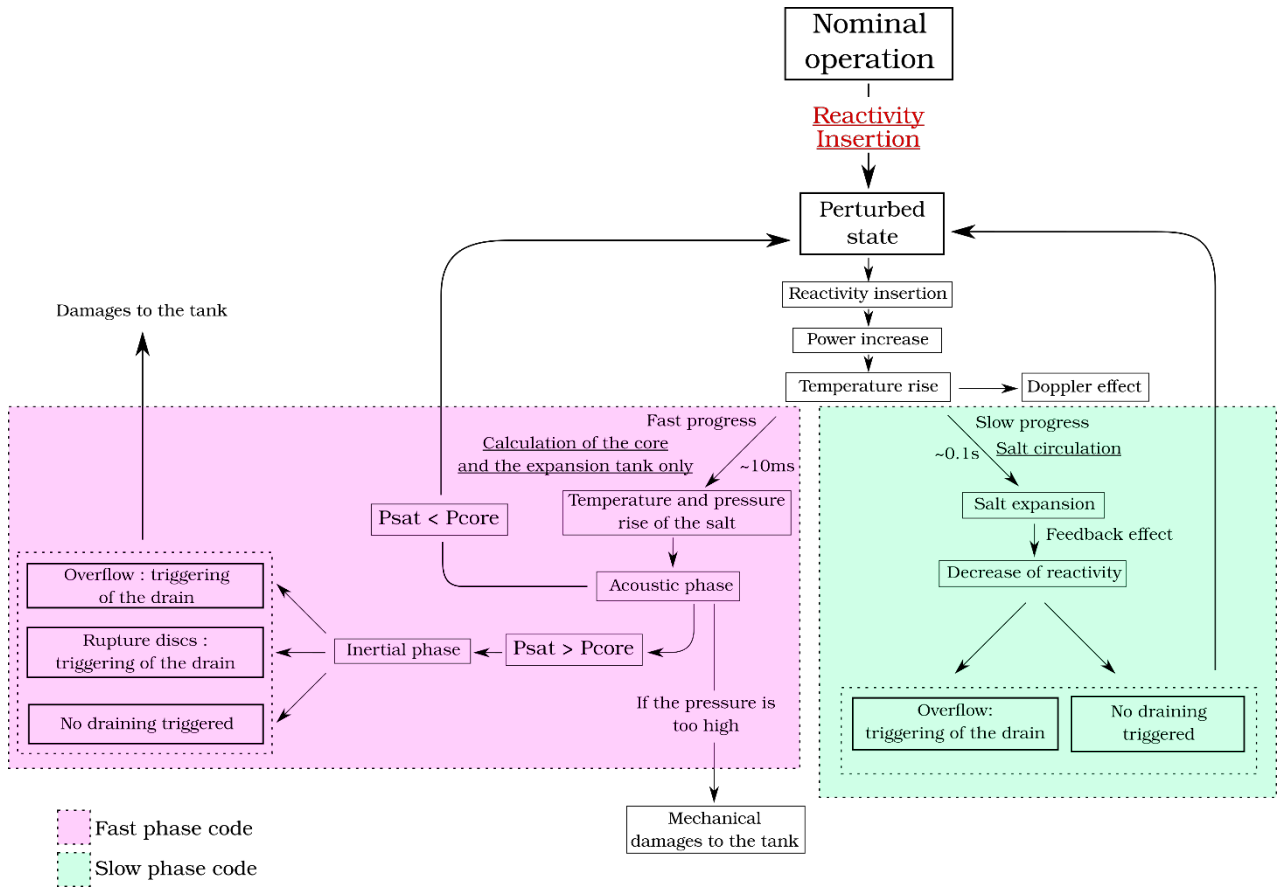AUTHOR et al.]

FIG 1 Phenomenological tree

But in the case of a fast temperature increase, the salt can't expand, and the pressure will increase in the core which lead to an acoustic phase and if the temperature rises higher than the vaporisation temperature, to an inertial phase. This is the fast phase of the transient. The acoustic phase models a pressure wave from the centre of the core to the expansion tank. If the bubbling is done in the core, the pressure increases and the bubbles of the treatment gas inside the salt collapse. These bubbles collapse leads to a positive feedback on reactivity In nominal operation, the salt has to be a bit more critical than expected because the bubbles are located at some position where the neutronic flux is high. When they collapse, fuel salt takes place of void where the neutron flux is high, which induces a higher number of fissions so a reactivity insertion. The pressure will decrease with the return of the relaxation wave. In the case where the temperature becomes higher than the vaporisation temperature, the salt will vaporise in the core, but this vaporisation is limited by the mechanical inertia of the liquid around the vapour.
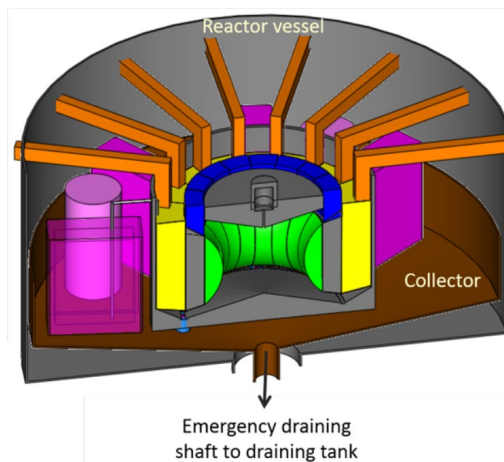

FIG. 2. Scheme of the MSFR [1]. The salt blanket is display in green and the heat exchangers in yellow. The critical zone is within the blanket, the expansion tank above the critical zone and the draining tank below the core; not display on this figure.

T.Le Meute, F.Bertrand, N.Seiler, E.Merle, D.Heuer

[Left hand page running head is author's name in Times New Roman 8 point bold capitals, centred. For more than two authors, write AUTHOR et al.]

Currently, these phenomena are not yet considered in most of the codes available to the authors calculation tools developed to study this kind of reactor, this explains why the transients presented are limited to slow heating without acoustic phase and vaporization. Our ultimate goal is thus the chaining of two codes (for small and large reactivity insertion) to calculate any kind of accidental scenarios that could lead to successive recriticalities. To model the behaviour of a MSFR system (see the scheme in Fig.2), we separate the core in elementary elements, which are considered as one-way flowing pipe axially meshed. The first part of this paper is devoted to the calculation method for temperature and velocity fields. This method can be applied knowing the salt flow at the pump that is why the second part will focus on the evolution of this flow during the transient. This method permits also to calculate the salt flow in the draining system.

1.   TEMPERATURE AND VELOCITY FIELD

In each pipe, the value of enthalpy per mass unit h [J/kg] and masse flow rate m [kg/s] are known and we dedicate the index e for the inlet and the index s for the outlet of the pipe. N_m will be the number of meshes in a pipe. These notations are summarized in Table.1.
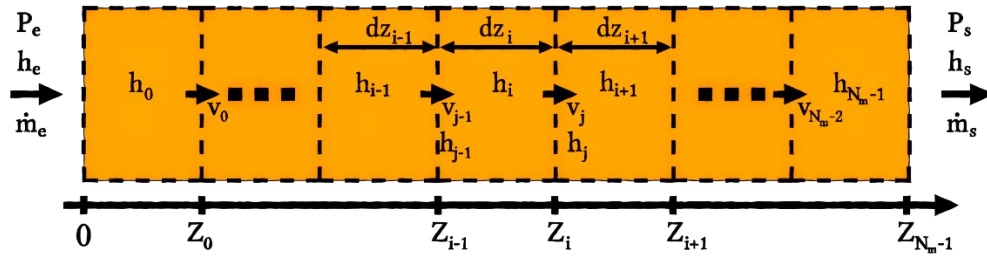

FIG 1 Mesh scheme for a pipe

For the calculation of the temperature evolution and the velocity of salt, we consider the balance equations of mass and enthalpy. These equations can be written:

$$\begin{cases} \dfrac{\partial}{\partial t}(\rho) + div(\rho\vec{v}) = 0 \\ \dfrac{\partial}{\partial t}(\rho h) + div(\rho h\vec{v}) = q \end{cases} \tag{1}$$

To solve these equations, the shifted volume finite method is used. The velocity of the salt is calculated on the surface between meshes and the temperature is calculated at the centre of the meshes. The index j is used for the velocity of the salt between the meshes i and i+1 as it is summarized in the scheme of Fig.3. By integrating the equation system (1) over a volume V_i (between Z_{i-1} and Z_i in Fig.3) we can write:

$$\begin{cases} \dfrac{\partial}{\partial t}(V_i\rho_i) + (\rho v S)_j - (\rho v S)_{j-1} = 0 \\ \dfrac{\partial}{\partial t}(\rho h) + (\rho h v S)_j - (\rho h v S)_{j-1} = P_i \end{cases} \tag{2}$$

Here, the convective terms can be linked to the finite different method, in the case of $S_j = S_{j-1}$: $(\rho v S)_j - (\rho v S)_{j-1} = V_i ((\rho v)_j - (\rho v)_{j-1})/dz_i$ which correspond to the discretization of the spatial derivative in one dimension. In the pipes, the direction of the flow is known, an upwind differencing scheme is used. With this scheme, the equation's system (2) can be written:

$$\begin{cases} \dfrac{\partial}{\partial t}(V_i\rho_i) + \rho_i(vS)_j - \rho_{i-1}(vS)_{j-1} = 0 \\ \dfrac{\partial}{\partial t}(V_i\rho_i h_i) + \rho_i h_i(vS)_j - \rho_{i-1}h_{i-1}(vS)_{j-1} = P_i \end{cases} \tag{3}$$

If i=0, $\rho_{i-1} = \rho_e$ and $h_{i-1} = h_e$. To simplify the notation, we introduce $m_{i-1} = \rho_{i-1}(Sv)_{j-1}$ and $m_i = \rho_i(Sv)_j$.
Or h and ρ are function of only one parameter, the temperature:

$$\begin{cases} h(T) = h_0 + \displaystyle\int_{T_0}^{T} C_p dx \\ \rho(T) = \rho_0(1 - \alpha(T - T_0)) \end{cases} \tag{4}$$

3

T.Le Meute, F.Bertrand, N.Seiler, E.Merle, D.Heuer

[Left hand page running head is author's name in Times New Roman 8 point bold capitals, centred. For more than two authors, write AUTHOR et al.]

With C_p [J.kg^{-1}] the heat capacity and α [K^{-1}] the expandability of the salt. We can then write the equation's system (3):

$$\begin{cases} V_i \dfrac{\partial \rho_i}{\partial T}(T_i)\dfrac{\partial T_i}{\partial t} + m_i - m_{i-1} = 0 \\ V_i \dfrac{\partial(\rho_i h_i)}{\partial T}(T_i)\dfrac{\partial T_i}{\partial t} + m_i h_i - m_{i-1}h_{i-1} = P_i \end{cases} \tag{5}$$

2.   EVOLUTION OF THE MASS FLOW RATE

The simplification of the MSFR fuel circuit in this work will be composed with pipes previously presented. A scheme of the modelling of the core is presented in Fig.4. In this work, a similar method as the one use in [2] will be used. Firstly from the impulsion balance equation in one dimension (the direction of the flow, noted z) will be evaluated as well as expression for the variation of pressure between the inlet and the outlet of each pipe:

$$\frac{\partial \rho v}{\partial t} + \frac{\partial \rho v^2}{\partial z} = -\frac{\partial p}{\partial z} + F \tag{6}$$

The function F corresponds to the pressure drop in the pipe (friction on the pipe surface: F [Pa.m^{-1}] = (f/2D$_H$) ρv^2 and change of direction of the flow. The second one will appear only after integration).
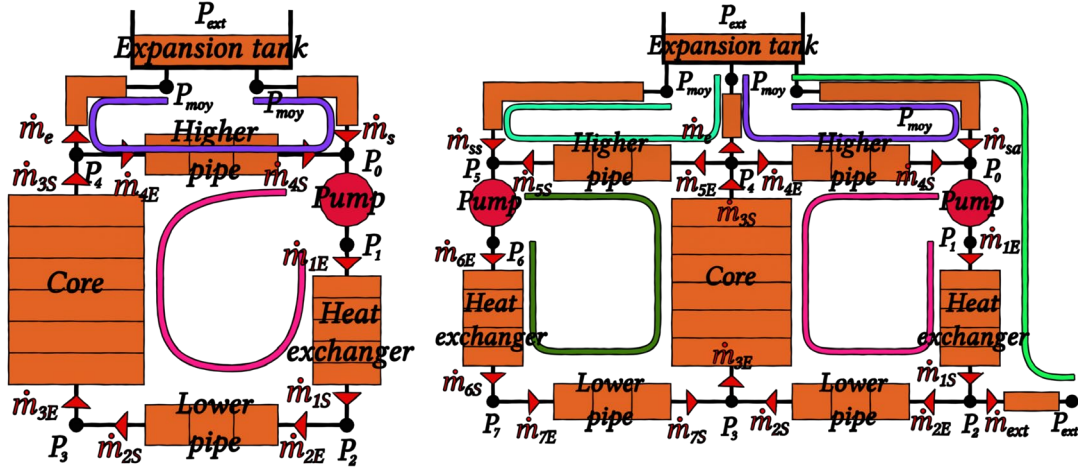

FIG 2 Scheme of the core meshed with pipes. Without draining (left) and with draining (right)

Again, considering $\rho vS = m$, the integration of equation (6) between the inlet and the outlet of the pipe permits to write:

$$\int_e^s \frac{\partial}{\partial t}\left(\frac{m}{S}\right)dz + \left[\frac{m^2}{\rho S^2}\right]_e^s = (P_e - P_s) + \int_e^s F dz \tag{7}$$

By deriving the equation system (5) we can show that the evolution of $\frac{dm_s}{dt}$ is linear with $\frac{dm_e}{dt}$, these coefficients will be note C and D such as:

$$\frac{dm_s}{dt} = C\frac{dm_e}{dt} + D \tag{8}$$

We can do the same for each $\frac{dm_i}{dt}$. And by considering that the evolution of $\frac{\partial m}{\partial t}$ for $z \in [Z_{i-1}, Z_i]$ is linear between $\frac{dm_{i-1}}{dt}$ and $\frac{dm_i}{dt}$, it's possible to integrate the integral term of the equation (7), which leads to write:

$$\frac{dm_e}{dt} = \frac{(P_e - P_s) + G}{H} \tag{9}$$

The equations governing the evolution of m$_{1e}$ the mass flow rate to the pump, m$_{6e}$ the mass flow rate to the pump in the sector there is no draining system (in case of draining), m$_e$ the mass flow rate at the entrance of the expansion tank, m$_{ext}$ the mass flow rate extracted by the draining system and x, a variable between 0 and 1, defined by:

4

T.Le Meute, F.Bertrand, N.Seiler, E.Merle, D.Heuer

[Left hand page running head is author's name in Times New Roman 8 point bold capitals, centred. For more than two authors, write
AUTHOR et al.]

$$m_{4e} = \frac{1-x}{N_a}(m_{3s} - m_e) \tag{10}$$

With N_a the number of sectors with draining system. The equation system to calculate the temporal evolution of these quantities are deriving by calculating the pressure difference between the lines drawn in Fig.4.

3.   NEUTRONICS

The neutronic model coupled to the previous thermal-hydraulic system is based on the model in [3]. This model is a point kinetic model improved to consider a spatial dimension. The equations for the evolution of N_n [m^{-3}] the neutron concentration and (C_i), the concentration of precursors of delayed neutrons are the followings:

$$\begin{cases} \dfrac{dN_n}{dt} = \dfrac{\rho_n - \beta}{\Lambda}N + \sum_{k=1}^{N_f} \lambda_k \dfrac{\iiint_{V_c} C_k(t,\vec{r})\varphi(\vec{r})d\vec{r}}{\iiint_{V_c} \varphi(\vec{r})^2 d\vec{r}} \\[3mm] \forall k \in \{1,\dots,N_f\}, \dfrac{\partial C_k}{\partial t} + div(C_k\vec{v}) = \dfrac{\beta_k}{\Lambda}N_n\varphi - \lambda_k C_k \\[3mm] \rho_n = \rho_{n,0} + \alpha_n(T_f - T_{ref}) \end{cases} \tag{11}$$

We consider that the flux and the adjoint flux are identical [3]. T_f is calculated as:

$$T_f = \iiint_{V_c} \varphi(\vec{r})T(\vec{r})d\vec{r} \tag{12}$$

The calculation scheme is the same as for temperature, in the upwind shifted volume finite method, the equations become, with the same notations than the ones used for temperature and velocity:

$$\begin{cases} \dfrac{dN_n}{dt} = \dfrac{\rho_n - \beta}{\Lambda}N + \sum_{k=1}^{N_f} \lambda_k \dfrac{\iiint_{V_c} C_k(t,\vec{r})\varphi(\vec{r})d\vec{r}}{\iiint_{V_c} \varphi(\vec{r})^2 d\vec{r}} \\[3mm] \forall k \in \{1,\dots,N_f\}, V_i\dfrac{\partial C_{i,k}}{\partial t} + C_{i,k}(vS)_j - C_{i-1,k}(vS)_{j-1} = \dfrac{\beta_k}{\Lambda}N_n\iiint_{V_i}\varphi(\vec{r})d\vec{r} - V_i\lambda_k C_k \\[3mm] \rho_n = \rho_{n,0} + \alpha_n(T_f - T_{ref}) \end{cases} \tag{13}$$

For the calculations, the coefficient for delay neutrons family are taken from [1] and the total thermal feedback coefficient is α_n = -8 pcm.K^{-1} as written in [3].

4.   RESULTS

The equations presented in the two previous parts of this article are solved with a Runge-Kutta of order 4 method. This method was chosen because it represents a good compromise between the stability and the ease of development. In the calculation tool, a steady-state is reached before starting the transient. The steady-state phase will be discussed further, this part focuses on the reactivity insertion transients.

4.1.   Study on the convergence of meshes

Before presenting results and discussing the behaviour of the calculation tool, a study about the convergence in meshes is presented. The transient calculated is a reactivity insertion of 1000 pcm in 1 s. The results are displayed in Fig.5.

T.Le Meute, F.Bertrand, N.Seiler, E.Merle, D.Heuer

[Left hand page running head is author's name in Times New Roman 8 point bold capitals, centred. For more than two authors, write AUTHOR et al.]
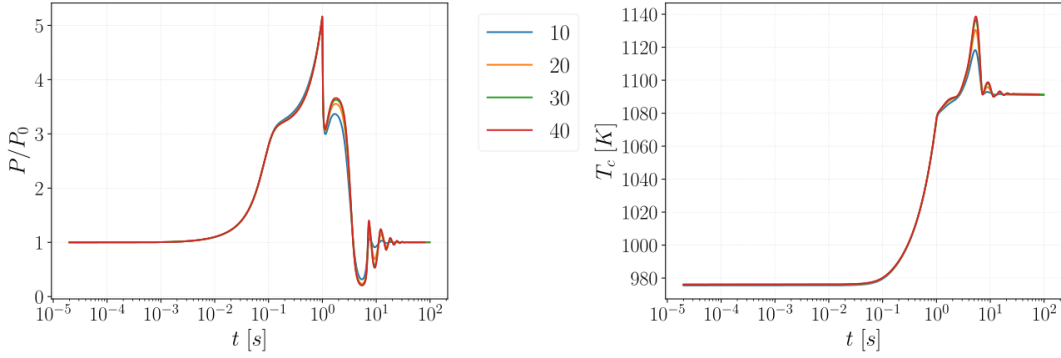
FIG 3 History of the normalized power and the temperature of the salt in the core for the insertion of 1000 pcm in 1 s. The different curves correspond to different numbers of meshes of the core.

The differences on these figures converge because the differences between the 30 meshes and the 40 meshes are really close. But choosing 20 meshes makes already a good approximation and accelerates the calculation, we thus selected this value in the following calculations.

4.2.   Reactivity ramp insertion without draining

The first realised transient is an external linear reactivity insertion of 1000 pcm in 1 s. The results of this transient are displayed in Fig.6. It can be noticed that the evolution of the reactivity follows the external reactivity inserted ρ_0 until the temperature begins to rise, at this point the reactivity is stabilised. The rapid increase of the temperature induces a decrease of the mass flow rate on the pump due to the expansion of the salt.
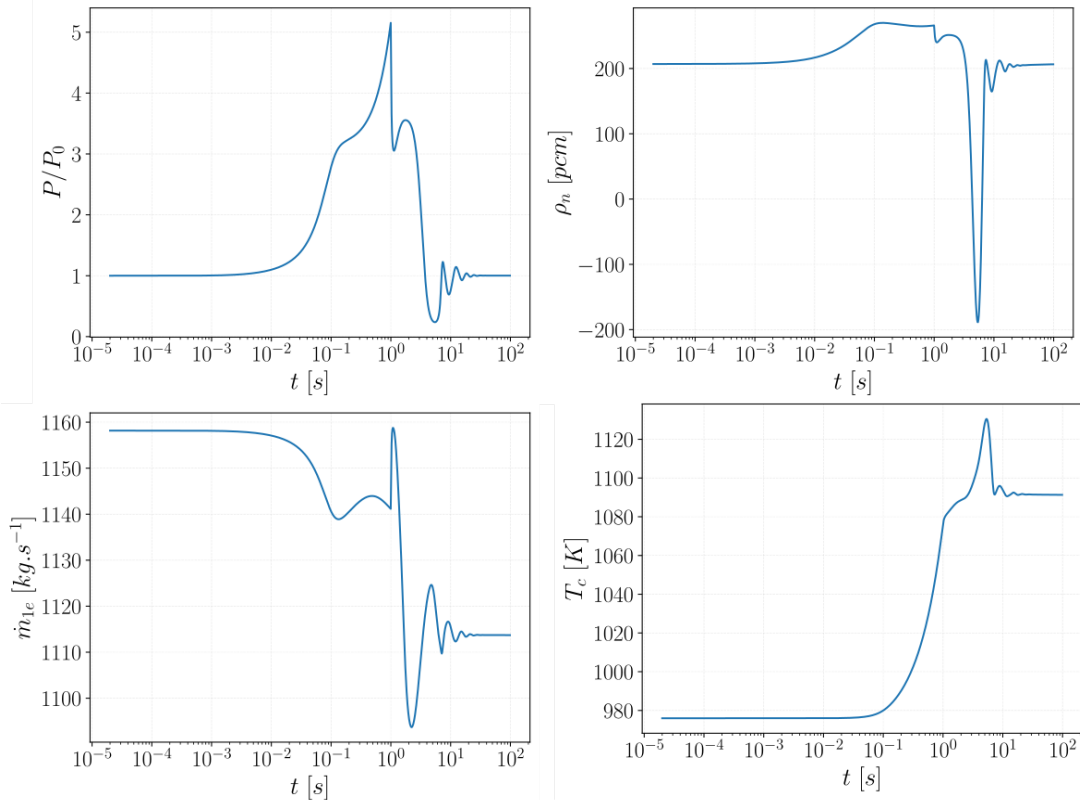

FIG 4 Evolution with time of the normalized power, reactivity, mass flow rate at the pump and mean temperature of the salt in the core for the insertion of 1000 pcm in 1 s.

4.3.   Reactivity ramp insertion with draining

T.Le Meute, F.Bertrand, N.Seiler, E.Merle, D.Heuer

[Left hand page running head is author's name in Times New Roman 8 point bold capitals, centred. For more than two authors, write
AUTHOR et al.]

The first simulated transient with draining is a linear external reactivity insertion of 1500 pcm in 1 s. The draining of the core is triggered by a fuse membrane, when the volume of the salt in the expansion tank exceeds the triggering volume V_t. The salt is in contact with the fuse membrane and the membrane takes t_t to melt. The melting of this membrane will actuate the draining by depressurization of gas volume. At the beginning of the calculation, the expansion tank is filled with 2 m³ of salt, the trigger volume is assumed to be $V_t = 2.5$ m³ and the trigger time $t_t = 5$ s. The results of these calculations are displayed in Fig.7. The first conclusion of these calculations is that, as expected, the fuel draining takes a longer time if the pressure drop in the draining system increases. This value was randomly chosen for these calculations. The design of the draining system has to be study in more detail to estimate the value of the pressure drop coefficient.
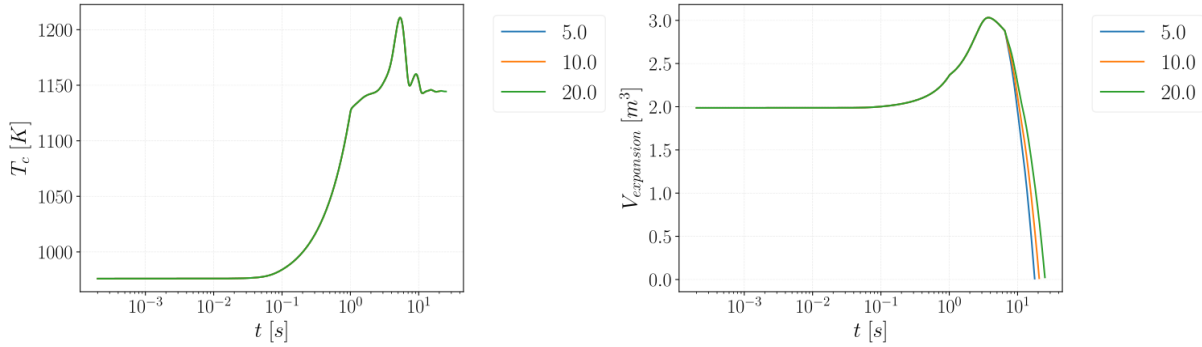

FIG 5 History of the mean core temperature of the salt and the volume in the expansion tank for the insertion of 1500 pcm in 1 s. The different curves correspond to the pressure drop constant in the draining system.

4.4. Reactivity step

The last calculation presents in this part is an insertion of a reactivity step, the results are displayed in Fig.8. During this transient, the power quickly increases and so does the temperature in the core to compensate this reactivity increase. The fast power increase induces a strong variation of the mass flow rate at the pump even if the pump is model as constant driving pressure. The exponential evolution of P is also plotted in Fig.8, the evolution of the power calculated by the calculation code follows closely this curve.
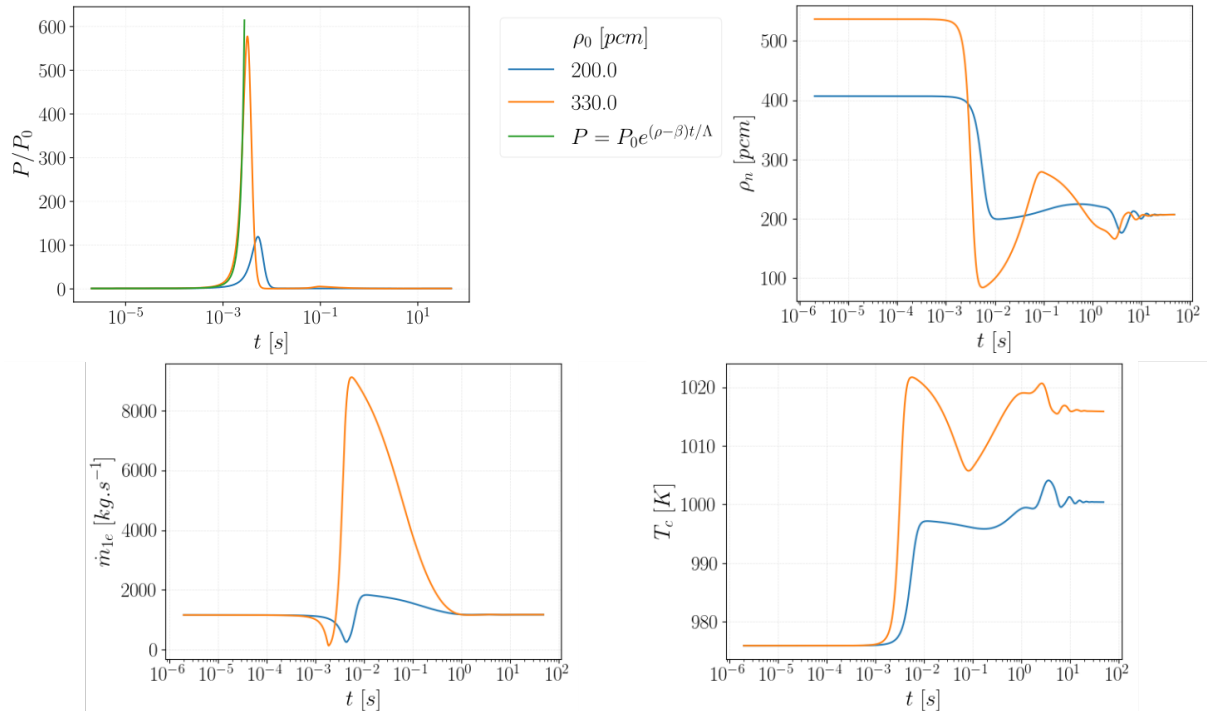

FIG 6 Evolution with time of the normalized power, reactivity, mass flow rate at the pump and mean temperature of the salt in the core for the insertion of a step of external reactivity. The different curves correspond to a different values of the external reactivity.

7

T.Le Meute, F.Bertrand, N.Seiler, E.Merle, D.Heuer

[Left hand page running head is author's name in Times New Roman 8 point bold capitals, centred. For more than two authors, write
AUTHOR et al.]

5. DISCUSSION ON THE LIMITS AND FUTURE IMPROVEMENTS OF THE CALCULATION TOOL

The calculation of a reactivity step permits to show one limit of this calculation code. The equations used in this tool are for incompressible flow, but as displayed in Fig.8, the value of power increases to a high level, ≈ 550 times the nominal power of the core. And the mean temperature of the core quickly increases, around 50 K in 4 ms which means that the temperature increase will probably induce a local pressure increase. This fast phase can't be calculated with this calculation tool but could be important because during reactivity transient, the temperature increase will not lead to the dilatation of salt. This phenomenon has strong consequences on the neutronic behaviour of the core because the total neutronic feedback effect considers the Doppler effect and the salt dilatation effect. In the fluoride version of the reactor, the value of the total neutronic feedback coefficient comes half from the Doppler effect and half from the density effect. Thus, the increase of temperature has to be twice higher if there is no thermal expansion to compensate the same inserted reactivity. For a chloride salt, the consequences can be much more severe because the Doppler effect is low (a few percentage of the total feedback coefficient).

Because this calculation tool does not permit to take into account this kind of physical phenomena, it is foreseen to model them with another tool. But to do this, the first objective it to find a criterion to quantify the importance of this phenomenon. During the propagation of a shock wave in a fluid, the speed of liquid behind the shock wave is evaluated as $v_{sw} = \frac{dP}{\rho_0 c_0}$ in [4] with dP the pressure increase owing to thermal dilatability between the shocked medium and the non-shocked medium. The criterion of transition between no-compressibility to compressibility is commonly $\frac{dP}{\rho_0 c_0^2} > 0.01$. For the previous calculations of reactivity step, the evolution of $\frac{dP}{\rho_0 c_0^2}$ is represented in the Fig.9. We notice that this criterion is roughly reached, in both transients and thus the fast pressure phases should be simulated in the future.
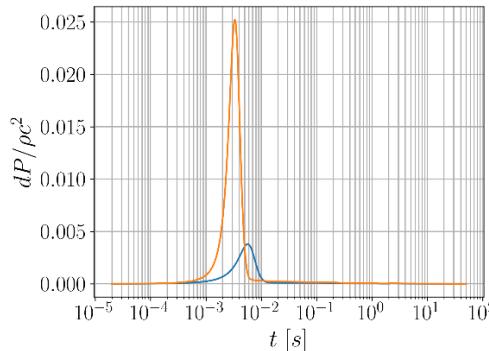

FIG 7 Evolution of $\frac{dP}{\rho_0 c_0^2}$ for the insertion of reactivity step.

Steady-state calculation:

As mentioned before in this article, the calculation tool is separated into two parts, the steady-state and the transient calculation. The evolution before reaching the steady-state calculation is displayed in Fig.10. The calculations show that the system oscillates before becoming stable. These oscillations are caused by the thermal disequilibrium at the beginning of the calculation and the limit condition which is a constant extracted power. The damping of these oscillations are due to the neutronic part of the calculation and probably a little from the diffusion of the numerical scheme. The power of the core follows the temperature of the salt: the power decreases when the salt gets warmer and increases when the salt gets colder. The conclusions on the convergence of the results with the number of meshes are quite the same than for the transient. The differences are not large except for the oscillating part.

T.Le Meute, F.Bertrand, N.Seiler, E.Merle, D.Heuer

[Left hand page running head is author's name in Times New Roman 8 point bold capitals, centred. For more than two authors, write AUTHOR et al.]
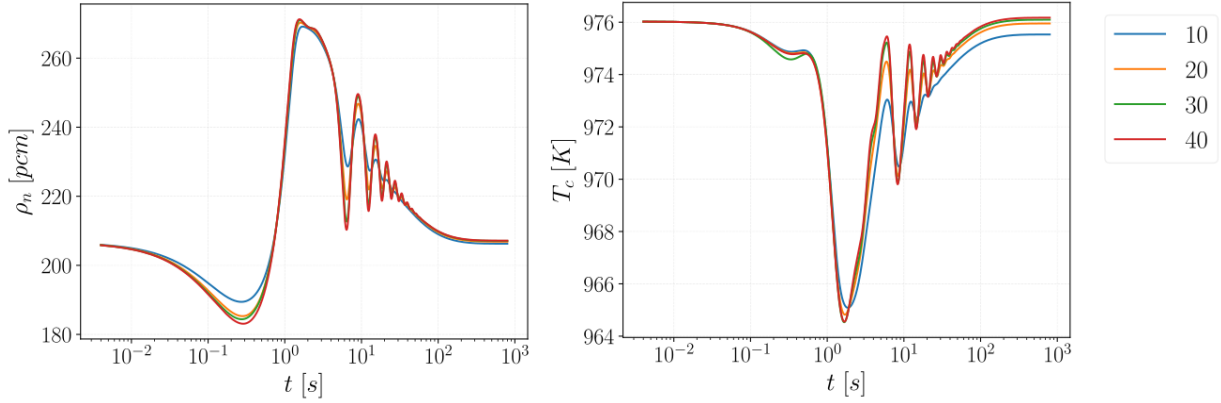
FIG 8 Evolution with time of the reactivity and mean temperature of the salt in the core for the steady-state calculation. The different curves correspond to the number of meshes in the core (from 10 to 40).

Other current limitations for the modelling:

In this calculation tool, the power extracted at the heat exchanger is constant which can be a limitation to simulate the return to the nominal state after the reactivity insertion. This has to be included in this calculation tool because the extracted power will change when the temperature of the salt change and this will balance the extracted power with the core power.

6.   CONCLUSIONS AND PERSPECTIVES

The objective of this work is to study the transient of reactivity insertion in a molten salt reactor and our studies are based on the MSFR. The transient were separated in two types of phases, the "slow" and the "fast" phase. In this paper was presented the first part of the calculation of a reactivity transient in a molten salt reactor: the transport part with the modelling of the full reactor. The equations and methods used were presented in the first part. These initial calculations are encouraging for this work of modelling reactivity transients and will enable to simulate some reactivity insertion transient in a MSFR. This calculation tool will be used to perform some studies of reactivity transient especially about the efficiency of the draining.

The limitations of these calculations were discussed in the previous part and some new components have to be added in this modelling to represent more accurately the physical phenomena in the reactor fuel circuit. This permits also to discuss about the fast phase modelling introduced in the previous part which will be part of our future work.

7.   AKNOWLEDGMENT

8.   NOTATIONS

ρ [kg.m^{-3}]	Density
h [J.kg^{-3}]	Mass enthalpy
v [m.s^{-1}]	Velocity
q [W.m^{-3}]	Power per unit volume
P_i [W]	Thermal power in the mesh i
V_c [m^3]	Volume of the core
V_i [m^3]	Volume of the mesh i

T.Le Meute, F.Bertrand, N.Seiler, E.Merle, D.Heuer

[Left hand page running head is author's name in Times New Roman 8 point bold capitals, centred. For more than two authors, write AUTHOR et al.]

S_j [m^2]	Surface between meshes i and i+1
T_i [K]	Temperature in the mesh i
T_f [K]	Temperature of the salt in the core integrated on the neutronic flux
T_{ref} [K]	Reference temperature for the calculation of reactivity
N_m	Number of meshes in a structure
N_f	Number of delay neutron family
N_n [m^{-3}]	Neutron population per unit volume
ρ_n [pcm]	Reactivity
$\rho_{n,0}$ [pcm]	External reactivity inserted
α_n [pcm.K^{-1}]	Total thermal neutronic feedback coefficient
(C_i) [m^{-3}]	Delayed neutron population concentration
(λ_i) [s^{-1}]	Decay constant of delayed neutron for each family
(β_i) [pcm]	Delayed neutron fraction for each family
φ	Neutronic flux normalized shape
ΔP [Pa]	Driving pressure of the pump
m_{1e} [kg.s^{-1}]	Mass flow rate through the pump or through the pump on a sector with draining system
m_{6e} [kg.s^{-1}]	Mass flow rate through the pump on a sector without draining system
m_e, m_{ext} [kg.s^{-1}]	Mass flow rate inlet of the expansion tank and in the draining system
F [Pa.m^{-1}]	Pressure drop function

Table 1. Used notations

REFERENCES

[1] Michel Allibert, Manuele Aufiero, Mariya Brovchenko, Sylvie Delpech, Véronique Ghetta, Daniel Heuer, A. Laureau, Elsa Merle-Lucotte, "Chapter 7 - Molten Salt Fast Reactors", Handbook of Generation IV Nuclear Reactors, Woodhead Publishing Series in Energy (2015)

[2] D. Gérardin, Développement de méthodes et d'outils numériques pour l'étude de la sûreté du réacteur à sels fondus MSFR. PhD thesis, Université Grenoble Alpes, 2018.

[3] J.-B. Droin, N. Marie, A. Bachrata, F. Bertrand, E. Merle, and J.-M. Seiler, "Physical tool for unprotected loss of flow transient simulations in a sodium fast reactor," Annals of Nuclear Energy, vol. 106, pp. 195–210, 2017.

[4] A. Laureau, Développement de modèles neutroniques pour le couplage thermohydraulique du MSFR et le calcul de paramètres cinétiques effectifs. PhD thesis, Université Grenoble Alpes, 2015.

[5] D.H.Cho, R.O.Ivins, and R.W.Wright, "A Rate-Limited Model of Molten-Fuel/Coolant Interactions : Model Development And Preliminary Calculations ," 1972.